JETIR.ORG ISSN: 2349-5162 | ESTD Year : 2014 | Monthly Issue
JOURNAL OF EMERGING TECHNOLOGIES AND INNOVATIVE RESEARCH (JETIR)
An International Scholarly Open Access, Peer-reviewed, Refereed Journal

Clipping Noise Mitigation in Optical OFDM System

MD.Yasmeen[1],G.Rohith[2],N.Vishnu[3],N.Chiranjeevi[4]

Assistant professor[1],Department Electronics and Communication Engineering, [2.3.4]Student, Department of Electronics and Communication Engineering, CMR Institute of Technology, Hyderabad, Telangana, India.501401

ABSTRACT

Orthogonal Frequency Division multiplexing(OFDM) is considered to be a promising technique against the multipath fading channel for wireless communications. However, OFDM faces PAPR problem which leads to power inefficiency in RF section of the transmitter. Tone injection (TI) mitigates the high peak-to average power ratio problem without incurring data rate loss or extra side information. In this project, a novel TI scheme that uses the clipping noise to find the optimal equivalent constellations is proposed. The proposed scheme achieves significant PAPR Reduction while maintaining low complexity.

Introduction

Recently, ocean exploration has attracted researchers' attention due to developments in military, industry, and scientific issues. Some of the most important applications of underwater wireless communications (UWC) include oceanography study, underwater surveillance, seafloor exploration, and monitoring, underwater oil pipe inspection, remotely operated vehicles (ROV), and sensor networks [1]-[5]. Although the dominant communications schemes used in underwater are still based mainly on the wireless technologies of radio frequency (RF) and acoustic (sonar), they suffer from low transmission data rate, limited bandwidth, high latency, and high attenuation which need to be addressed [6], [7].

Orthogonal frequency division multiplexing (OFDM) has been attracting substantial attention due to its excellent performance under severe channel condition. The rapidly growing application of OFDM includes Wi-MAX, DVB/DAB and 4G wireless systems.

Literature Review

Orthogonal frequency division multiplexing (OFDM)networking and broadband internet access

Orthogonal frequency-division multiplexing (OFDM), essentially identical to coded OFDM (COFDM) and discrete multi-tone modulation (DMT), is a frequency-division multiplexing (FDM) scheme used as a digital multi-carrier modulation method. A large number of closely-spaced orthogonal sub-carriers are used to carry data. The data is divided into several parallel data streams or channels, one for each sub-carrier. Each sub-carrier is modulated with a conventional modulation scheme (such as quadrature amplitude modulation or phase-shift keying) at a low symbol rate, maintaining total data rates similar to conventional single-carrier modulation schemes in the same bandwidth.

OFDM has developed into a popular scheme for wideband digital communication, whether wireless or over copper wires, used in applications such as digital television and audio broadcasting, wireless communications.

Proposed method

The limited bit resolution of the DAC and ADC is one of the major implementation issues in O-OFDM systems.It can cause signal distortion, as they introduce quantization noise to the system. Clipping the signal is a possiblesolution that reduces the signal high peaks and allows reducing the dynamic range of the DAC and ADC at theexpense of BER degradation, due to the appearance of clipping noise.

Block diagram:

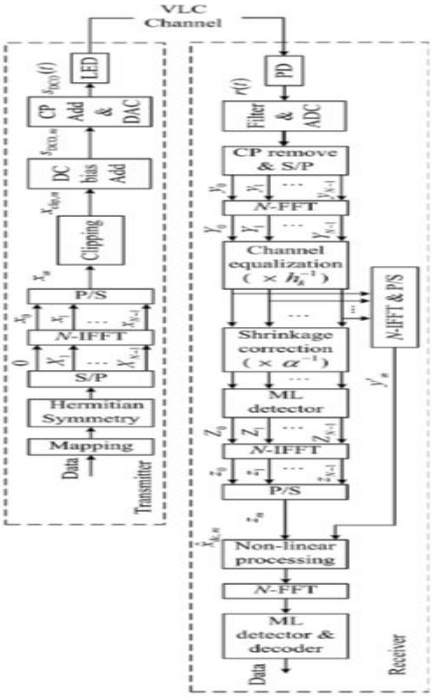

System Overview:

The input data is parallelized and mapped into BPSK or M-PAM format. Then the symbols are fed into a FHT of N points. A cyclic prefix (CP) can be added to the signal to compensate the intersymbol interference (ISI) [3].Then the modulated signal is serialized. Finally, it is symmetrically clipped and digital-to-analog converted.

Illustrates the schematic block diagram of the proposed DCO-OFDM UOWC system the with RCF method which is explained comprehensively as follows. The goal is to compare its performance with the DCOOFDM system without the RCF method under the same conditions. A. Transmitter At the Tx, a random data bit stream {In} is mapped onto the QAM format. Then, the modulated symbols are applied to the serial to parallel (S/P) converter. The pilot insertion block is considered to provide channel estimation at the Rx. Then, the signal is extended by inserting $N(L-1)$ zeros in its middle, resulting in the trigonometric interpolation of the time domain signal, where L is the oversampling factor [8]. The oversampled signal is passed through an LN-point inverse fast transform (IFFT) block generating the oversampled time-domain OFDM signal followed by the parallel to serial (P/S) converter, which is represented as: $x[n] = 1\ \sqrt{LN}\ \sum X[k]e\ j\ 2\pi k\ \Delta f\ n\ LN\ LN-1\ 0$ $n = 0, 1, \ldots, LN\text{-}1$, (1) As a result of intensity modulation/direct detection (IM/DD), the transmitted signal must be non-negative and real. Therefore, the Hermitian symmetry constraint is imposed to acquire a real-valued signal, as given by [23]: $\bar{x}HS = [0, xCF[1], xCF[2], \ldots, xCF\ [\ LN\ 2-1], 0, xCF * [\ LN\ 2\ 1], \ldots, xCF * [2], xCF * [1]\ ]$ (2) where $(.) *$ is the complex conjugate. A cyclic prefix (CP) is then prepended to each OFDM signal for eliminating the ISI and inter-block interactions (IBI) [12]. Following scaling of the CP added signal $xCP[n]$, we have: $Is\ [n] = \lambda s \times xCP[n]$, (3) where the scaling factor λs due to the limited dynamic range of the LED is defined as [9]: $\lambda s = MI \times Imax\ (MI+1)\times\max(xCP[n])$, (4) Here $Imax = Ib + 0.5\ IPP$ is the maximum value of Iin, Ib is the DC-bias current, IPP is the peak-to-peak current, and MI is the modulation index, which is defined as: $MI = IPP- IPP\ Ib$, (5) Then, following the digital to analog converter, a direct current (DC)-bias Ib is added to the time domain (TD) discrete scaled signal $Is\ [n]$ to make it non-negative prior to IM of the light source and transmission over the underwater channel as follows: $Iin(t) = Is\ (t) + Ib$, (6) At last, it is fed to drive the LED by convolving with the LED impulse response which is characterized as a first-order low pass Butterworth filter, given by [9]: $hLED[n] = \exp[-2\pi fLEDn]$, (7) where $fLED$ is the 3-dB cut-off frequency of the LED. Note, the PAPR is calculated from the L-times oversampled TD signal samples $x[m]$ as [19]: $PAPR\{x[m]\} = max0\leq t\ \leq NL-1\ |x[m]|\ 2\ E\ [|x[m]|\ 2\ ]$, (8) where $E\{.\}$ is the expectation operator. The complementary cumulative distribution function (CCDF), defined as CCDF $(PAPR) = \mathrm{P}\ \{PAPR > PAPR0\ \}$, is utilized to appraise the PAPR reduction performance. The target value of PAPR is designated as $PAPR0$ [10].

Three basic attributes of emitted photons include photon's weight, position in Cartesian coordinates (x, y, z), and transmission direction (characterized by polar θ and azimuthal angle φ). Photons interacting with particles in the water experience a change of direction and loss due to both scattering and absorption which can be evaluated by absorption coefficient, $a(\lambda)$, and scattering coefficient, $b(\lambda)$, respectively. The basic rules of this approach are summarized as follows [11], [12]. The initial photon's position is equal to the Tx position which is considered (0, 0, 0) in this study. The angle of θ and φ are chosen randomly between [- θmax, $\theta\ max$] and B. Noursabbaghi et al. 304 J. Electr. Comput. Eng. Innovations, 11(2): 301-310, 2023 [0, 2π] with uniform distributions, respectively, where θmax is the maximum initial divergence angle. The direction vector (μx, μy, μz) for each photon is equal to (sin θ cos φ , sin θ sin φ , cos θ). The scattering coefficient is considered to study the effect of multiple scattering which is defined by the integral of the spectral volume scattering function (VSF) over all directions as: $b(\lambda) = \int \beta(\theta, \lambda)\ d\Omega = 2\pi \int \beta(\theta, \lambda) \sin\theta\ d\theta\ \pi\ 0\ 4\pi\ 0$, (9) where $\beta(\theta, \lambda)$ is the VSF and $d\Omega$ is the solid angle centered on θ. Finally, the whole attenuation coefficient of spectral light beam is defined as, $c(\lambda) = a(\lambda) + b(\lambda)$. Note, a,b, and c are in units of m-1 . In addition, the angular probability distribution of the scattered photons at a given wavelength, known as the scattering phase function (SPF), is given by: $\tilde{\beta}(\theta, \lambda) = \beta(\theta,\lambda)\ b(\lambda)$, (10) Typically, the Henyey-Greenstein (HG) phase function is used to describe the SPF of dispersive medium such as water and atmosphere with the expression as: $\tilde{\beta}(\theta) = 1- g\ 2\ 4\pi(1+ g2-2g\cos\theta)\ 3/2$, (11) where g is the average cosine of θ in all scattering directions and almost equals 0.924 for all water types. At first and before any interactions, the photon passes a certain distance called the step size (Δs): $\Delta s = -\log \xi\ s\ c(\lambda)$, (12) where $\xi\ s$ is a uniform random variable between [0,1]. After that, the new coordinates of the photon's position are updated according to: $\acute{x} = x + \mu x \Delta s$, $\acute{y} = y + \mu y \Delta s$, $\acute{z} = z + \mu z \Delta s$, (13) The interaction of the photon with the scattering point leads to energy loss and deviation of the photon from the transmission direction. Therefore, the photon's energy level (weight) is updated by: $WPost = (1 - b\ c\ )\ WPre$, (14) where $WPost$ and $WPre$ represent the weights after and before the interaction, respectively. The new azimuth ($\acute{\varphi}$) and elevation ($\acute{\theta}$) angles also need to be calculated due to changing the photon transmission direction after the scattering point, as follows: $R = 2\pi \int \tilde{\beta}(\theta) \sin\theta\ d\theta\ \acute{\theta}\ 0$, (15) $\acute{\varphi} = 2\pi R$, (16) where R is a uniform random variable between [0, 1]. Then, from (15), $\acute{\theta}$ can be

obtained as: cos $\acute{\theta}$ = 1 2g [1 + g 2 − (1− g 2 1−g+2gR) 2]. (17) Finally, the new transmission direction vector can be calculated as [26]: $\mu\acute{x}$ = −μy sin $\acute{\theta}$ cos$\acute{\varphi}$+ μx(cos $\acute{\theta}$ +sin $\acute{\theta}$ sin$\acute{\varphi}$), $\mu\acute{y}$ = − μx sin $\acute{\theta}$ cos$\acute{\varphi}$+ μy(cos $\acute{\theta}$ + sin $\acute{\theta}$ sin $\acute{\varphi}$), $\mu\acute{z}$ = −(μx 2 + μy 2) sin $\acute{\theta}$ sin$\acute{\varphi}$ /μz + μz cos $\acute{\theta}$, (18) At the Rx side, a photon can be detected when its position and the arrival angle are within the Rx's aperture and Field of View (FOV) and its weight is higher than the threshold level. The process of photon scattering continues until the photon is received at the PD or disappeared by losing all its weight. The threshold weight at the PD is assumed 106 in this study. C. Receiver At the Rx side, the received signal is detected by an optical Rx composed of a single PD and a trans-impedance amplifier (TIA). The regenerated electrical received signal is given by: $y(t) = s(t) * hc\ (t) + n(t)$, (19) where $n(t)$ is the additive white Gaussian noise with the power $Pn = N0B$Rx, $N0$ is the noise power. Note, spectral density, and BRx is the bandwidth of the Rx. $n(t)$ is mostly dominated by the ambient light induced shot noise. Then, the received signal is amplified and converted to a parallel signal via the S/P block. Following CP removal, an N-point FFT block is employed to transform the TD signal $y[n]$ to the Frequency Domain (FD) signal $Y[k]$. The upper half of the signal is removed due to the use of Hermitian symmetry at the Tx side and then the least square (LS) method is utilized to calculate the complex-valued channel frequency response (CFR) based on pilot symbols, as follows: $Hp\ (m) = Yp(m)\ Xp(m)$, $m = 1, \ldots, Np$ (20) where m is the number of pilot sub-carrier, Np is the number of pilots in one OFDM symbol, $Yp\ (m)$ is the received pilot symbol that are extracted from every eight subcarriers of the received OFDM signal, and $Xp\ (m)$ is the transmitted pilot symbol. Then, linear interpolation is performed to compute the CFR function on the remaining subcarriers as: $H[(m − 1)]L + \ell] = Hp\ (m) + 1\ L\ [Hp\ (m + 1) − Hp\ (m)]$, $\ell = 1, \ldots, L$ (21) where $L = 8$ is the distance in subcarriers between two consecutive pilots. A one-tap frequency-domain equalizer (FDE) with the minimum mean square error (MMSE) method is used to compensate for the channel deficiencies. The MMSE coefficients are calculated as follows: $Ck\ MMSE = H\acute{}\ k * Hk\ H\acute{}\ k *+1/\gamma$, (22) where k is the number of subcarriers, and γ is the signal to noise ratio (SNR). So, the decision variable is calculated as: PAPR Reduction in OFDM UOWC System Employing Repetitive Clipping and Filtering (RCF) Method J. Electr. Comput. Eng. Innovations, 11(2): 301-310, 2023 305 $S\acute{}\ k = Ck\ MMSE\ Y[k]$, (23) Finally, $S\acute{}\ k$ is converted to a serial data stream using a parallel-serial (P/S) block prior to QAM demodulation [13].

PAPR in OFDM

OFDM is a powerful modulation technique being used in many new and emerging broadband communication systems.

Advantages:

1. Robustness against frequency selective fading and time dispersion.
2. Transmission rates close to capacity can be achieved.
3. Low computational complexity implementation (FFT).

Drawbacks:

1. Sensitivity to frequency offset.
2. Sensitivity to nonlinear amplification.
3. Compensation techniques for nonlinear effects
4. Linearization (digital predistortion).
5. Peak-to-average power ratio (PAPR) reduction.
6. Post-processing.

Clipping Noise Mitigation in OFDM Systems

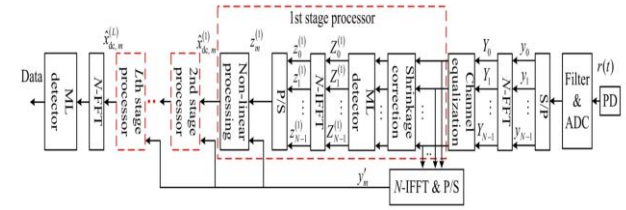

Clipping Noise Mitigation Algorithm

C. Clipping Noise Mitigation Algorithm

The clipping noise mitigation algorithm is shown in Fig. 1 and operates as follows:

1) The signal received by the photodetector (PD) is first filtered, converted from analog to digital and input to an FFT to give, $\mathbf{Y} = [Y_0, Y_1, \ldots, Y_{N-1}]$.
2) The elements of $\mathbf{Y}$ are equalized using h_k, the channel gain for each subcarrier, to give $Y'_k = h_k^{-1} Y_k$, which is then converted back to the discrete time domain to give y'_m.
3) The shrinkage is then corrected to give $\tilde{Y}_k = \alpha^{-1} Y'_k$.
4) $\tilde{Y}_k$ is then input into a ML detector to give output $Z_k = \underset{M \in \{M-QAM\}}{\arg\min} \left\| \tilde{Y}_k - M \right\|^2$.
5) An IFFT then converts Z_k into the time domain sequence, z_m. Note that in general the samples in $\mathbf{z} = [z_0, z_1, \ldots, z_{N-1}]$ will have both positive and negative values.
6) y'_m and z_m are used to generate a new time domain sequence, $\hat{x}_{\mathrm{dc},m}$, which is used to estimate $x_m + B_{\mathrm{DC}}$. It is generated by using the positive values of y'_m combined with the negative values of z_m for the samples where y'_m is negative or zero:

$$\hat{x}_{\mathrm{dc},m} = \begin{cases} y'_m, y'_m > 0 \\ z_m, y'_m \le 0. \end{cases} \quad (7)$$

Results

The CCDF function is used to evaluate the PAPR performance of 4-QAM DCO OFDM UOWC system with RCF method for a range of Clipping Ratio (CR) values. The clipping and filtering level, depth, and the number of subcarriers is one, 5 m, and 1024, respectively. The CCDF of PAPR is defined as CCDF (PAPR) = P (PAPR, respectively > $PAPR0$) where $PAPR0$ is the target PAPR value. It is clearly shown that utilizing the RCF method leads to the PAPR reduction up to ~4 dB, at CCDF of 10-2 and CR =4 compared with the original signal. In addition, it can be seen that the CCDF of PAPR can be remarkably reduced by decreasing CR. The best PAPR reduction is achieved for the lowest CR = 0.4 which is 6.9 and 7.35 dB at CCDF = 10-2 and CCDF = 10-3 , respectively, compared with the original signal.

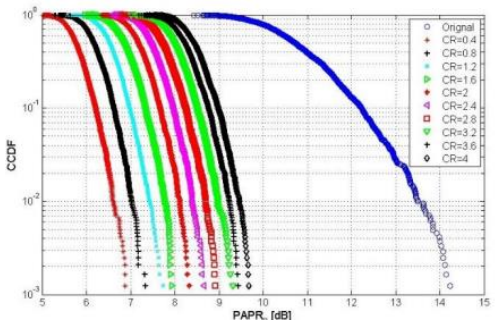

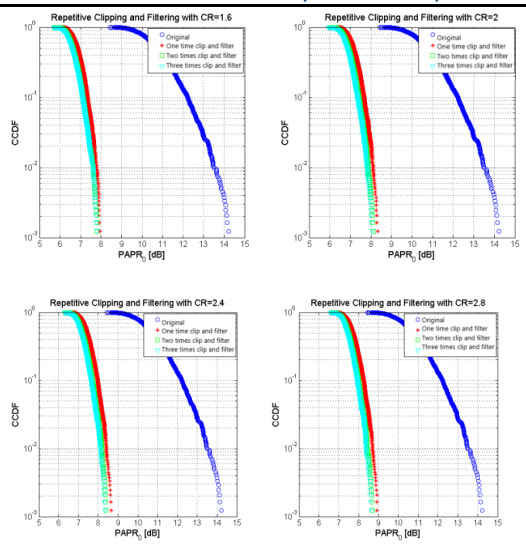

The CCDF performance is also examined when the clipping and filtering levels are 2 and 3 times at the CR of 1.6, 2, 2.4, and 2.8, as shown in Fig. 4. For example, for three times clipping and filtering scenario, the results demonstrate that at CCDF of 10-2 , the PAPR gains for the CR = 1.6, 2, 2.4, 2.8 are equal to 7.60, 7.85, 8.19, and 8.41 dB, respectively. The system BER and EVM performances are also evaluated for different CRs in a 4-QAM DCO OFDM system using RCF method. As can be seen in Fig. 5, by increasing the gain of CRs both BER and EVM performances of the system are improved.

ACKNOWLEDGEMENTS

We are extremely grateful to Dr.M.JangaReddy, Director, Dr.B.Satyanarayana, Principal and Dr.K.Niranjan Reddy, Head of Department ,Electronics and Communication Engineering, CMR Institute of Technology for their inspiration and valuable guidance during the entire duration. We are extremely thankful to our guide MS.MD.Yasmeen, Assistant professor , ECE , CMR Institute of Technology for her constant guidance, encouragement and moral support throughout the project.

REFERENCES

[1] A. K. Jain and A. Ross, Handbook of Biometrics. Springer, 2008,

Introduction to biometrics, pp. 1–22.

[2] C. Rathgeb and A. Uhl, “Attacking iris recognition: An efficient hillclimbing technique,” in IEEE/IAPR International Conference on Pattern

Recognition (ICPR), 2010, pp. 1217–1220.

[3] ——, “Statistical attack against iris-biometric fuzzy commitmentschemes,”

in IEEE Computer Society Conference on Computer Vision and Pattern

Recognition Workshops (CVPRW), 2011, pp. 23–30.

[4] J. Galbally, J. Fierrez, and J. Ortega-garcia, “Vulnerabilities in biometric

systems: Attacks and recent advances in liveness detection,” Database,vol.

1, no. 3, pp. 1–8, 2007, available at http://atvs.ii.uam.es/files/2007 SWB VulnerabilitiesRecentAdvances Galbally.pdf.

[5] N. K. Ratha, J. H. Connell, and R. M. Bolle, “An analysis of minutiae

matching strength,” in International Conference on Audio-and VideoBased Biometric Person Authentication, 2001, pp. 223–228.

[6] W. Robson Schwartz, A. Rocha, and H. Pedrini, “Face spoofing detection

through partial least squares and low-level descriptors,” in IEEE Int. Joint

Conference on Biometrics (IJCB), 2011, pp. 1 –8.

[7] D. Yi, Z. Lei, Z. Zhang, and S. Li, “Face anti-spoofing: Multi-spectral

approach,” in Handbook of Biometric Anti-Spoofing, ser. Advances in

Computer Vision and Pattern Recognition, S. Marcel, M. S. Nixon, andS.

Z. Li, Eds.S. Z. Li, Eds. Springer London, 2014, pp. 83–102.

[8] L. Ghiani, D. Yambay, V. Mura, S. Tocco, G. Marcialis, F. Roli, and S.

Schuckcrs, “Livdet 2013 – fingerprint liveness detection competition,” in

International Conference on Biometrics (ICB), 2013, pp. 1–6. [Online].

Available: http://prag.diee.unica.it/fldc/

[9] W. Zhang, S. Shan, W. Gao, X. Chen, and H. Zhang, “Local gabor binary

pattern histogram sequence (lgbphs): a novel non-statistical modelfor face

representation and recognition,” in IEEE Int. Conference on Computer

Vision (ICCV), vol. 1, 2005, pp. 786–791.

[10] G. L. Marcialis, A. Lewicke, B. Tan, P. Coli, D. Grimberg,A.

Congiu, A. Tidu, F. Roli, and S. A. C. Schuckers, "Livdet 2009–first

international fingerprint liveness detection competition," in Int. Conference

on Image Analysis and Processing (ICIAP), ser. Lecture Notes in Computer

Science, P. Foggia, C. Sansone, and M. Vento, Eds., vol. 5716. Springer,

2009, pp. 12–23. [Online]. Available: http://prag.diee.unica.it/LivDet09

[10] J. Galbally, F. Alonso-Fernandez, J. Fierrez, and J. Ortega-Garcia, "A high

performance fingerprint liveness detection method based on qualityrelated

features," Future Generation Computer Systems, vol. 28, no. 1, pp. 311–

321, 2012.

[11] D. Yambay, L. Ghiani, P. Denti, G. Marcialis, F. Roli, and S. Schuckers,

"Livdet 2011 – fingerprint liveness detection competition," in IAPR Int.

Conference on Biometrics (ICB), 2012, pp. 208–215. [Online]. Avail- able:

http://people.clarkson.edu/projects/biosal/fingerprint/index.php